JACS
JOURNAL OF THE AMERICAN CHEMICAL SOCIETY
Article
pubs.acs.org/JACS

Photoinduced Charge Transfer and Acetone Sensitivity of Single-Walled Carbon Nanotube–Titanium Dioxide Hybrids

Mengning Ding,[†,‡] Dan C. Sorescu,[†] and Alexander Star*[,†,‡]

[†]United States Department of Energy, National Energy Technology Laboratory, Pittsburgh, Pennsylvania 15236, United States
[‡]Department of Chemistry, University of Pittsburgh, Pittsburgh, Pennsylvania 15260, United States

Supporting Information

ABSTRACT: The unique physical and chemical properties of single-walled carbon nanotubes (SWNTs) make them ideal building blocks for the construction of hybrid nanostructures. In addition to increasing the material complexity and functionality, SWNTs can probe the interfacial processes in the hybrid system. In this work, SWNT–TiO_2 core/shell hybrid nanostructures were found to exhibit unique electrical behavior in response to UV illumination and acetone vapors. By experimental and theoretical studies of UV and acetone sensitivities of different SWNT–TiO_2 hybrid systems, we established a fundamental understanding on the interfacial charge transfer between photoexcited TiO_2 and SWNTs as well as the mechanism of acetone sensing. We further demonstrated a practical application of photoinduced acetone sensitivity by fabricating a microsized room temperature acetone sensor that showed fast, linear, and reversible detection of acetone vapors with concentrations in few parts per million range.

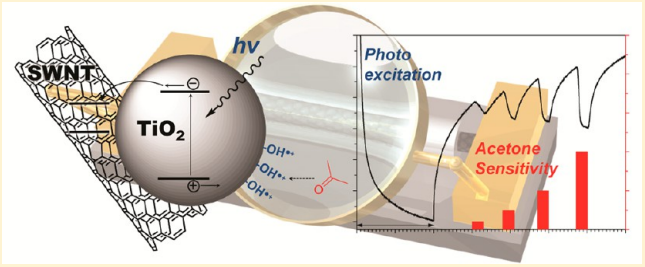

INTRODUCTION

Considerable research efforts have been recently devoted to develop novel hybrid nanostructures with increased complexity and expanded functionality that could benefit nanotechnology-based electronics,[1] medicine,[2−4] catalysis,[5,6] energy generation,[7,8] and sensors.[4,9−12] For example, titanium dioxide (TiO_2) has been combined with carbon nanotubes (CNTs) to improve the TiO_2 performance in photovoltaics[7] and photocatalysis.[13] Incorporation of CNTs brings certain potential advantages. First, the high conductivity of CNTs could provide effective electron pathways, therefore increase the electron diffusion length and prevent the electron–hole recombination.[7,13−15] Second, the one-dimensional (1-D) morphology of CNTs could serve as a template[16−18] to regulate the growth of TiO_2 into 1-D structures, while 1-D morphology[19−24] and core/shell architecture[25,26] could both lead to enhanced electronic transport and result in improved efficiency of photocatalysis or photovoltaic devices. The third advantage relates specifically to single-walled carbon nanotubes (SWNTs). Due to their unique optical and electrical properties that are sensitive to electron donation or acceptance, SWNTs could be employed as spectroscopic[12,27−31] or electrical[10,31−33] probes in a hybrid system to elucidate the underlying charge transfer and electronic interaction at the interface. Moreover, the ease of fabrication and the high performance of SWNT-based semiconductor devices allow the utilization of SWNT-based hybrid materials in real-world applications, such as chemical sensing.[10−12] In this work, we demonstrate the unique electrical behavior of SWNT–TiO_2 hybrid systems upon photoexitation and chemical exposure, through which their interfacial electronic coupling, charge separations, and photocatalytic activities can be successfully probed. In addition, we report a SWNT–TiO_2 nanohybrid with core/shell structure for the room-temperature detection of acetone vapors at ppm concentrations, which offers promising clinical applications (e.g., diagnostic tools) as concentration of breath acetone has long been correlated with ketoacidosis and the blood sugar level in case of diabetes.[34,35] Density functional theory (DFT) calculations have also been applied here to further study the electronic coupling of TiO_2 and SWNTs and to rationalize the underlying mechanism of acetone sensitivity.

RESULTS AND DISCUSSION

Synthesis of SWNT–TiO_2 Hybrids with Core/Shell Morphology. Oxidized SWNTs (o-SWNTs, containing surface oxygen functional groups between 1.0 and 3.0 atomic %)[36] were purchased from Carbon Solutions, Inc. and used as received. The growth of a TiO_2 layer over individual SWNT was achieved through a two-step sol–gel synthesis approach, as illustrated in Figure 1a. Carboxyl or hydroxyl groups on the surface of o-SWNTs first reacted with titanium(IV) isopropoxide ($Ti(O^iPr)_4$), which was used as the TiO_2 precursor. The grafted $-O-Ti(O^iPr)_3$ underwent further hydrolysis and condensation steps upon addition of water. This sol–gel process initiated from the surface of o-SWNTs produced a one-dimensional core/shell structure. Transmission electron microscopy (TEM) images (Figure 1b) illustrated the morphol-

Received: March 21, 2013
Published: May 21, 2013

dx.doi.org/10.1021/ja402887v | J. Am. Chem. Soc. 2013, 135, 9015−9022

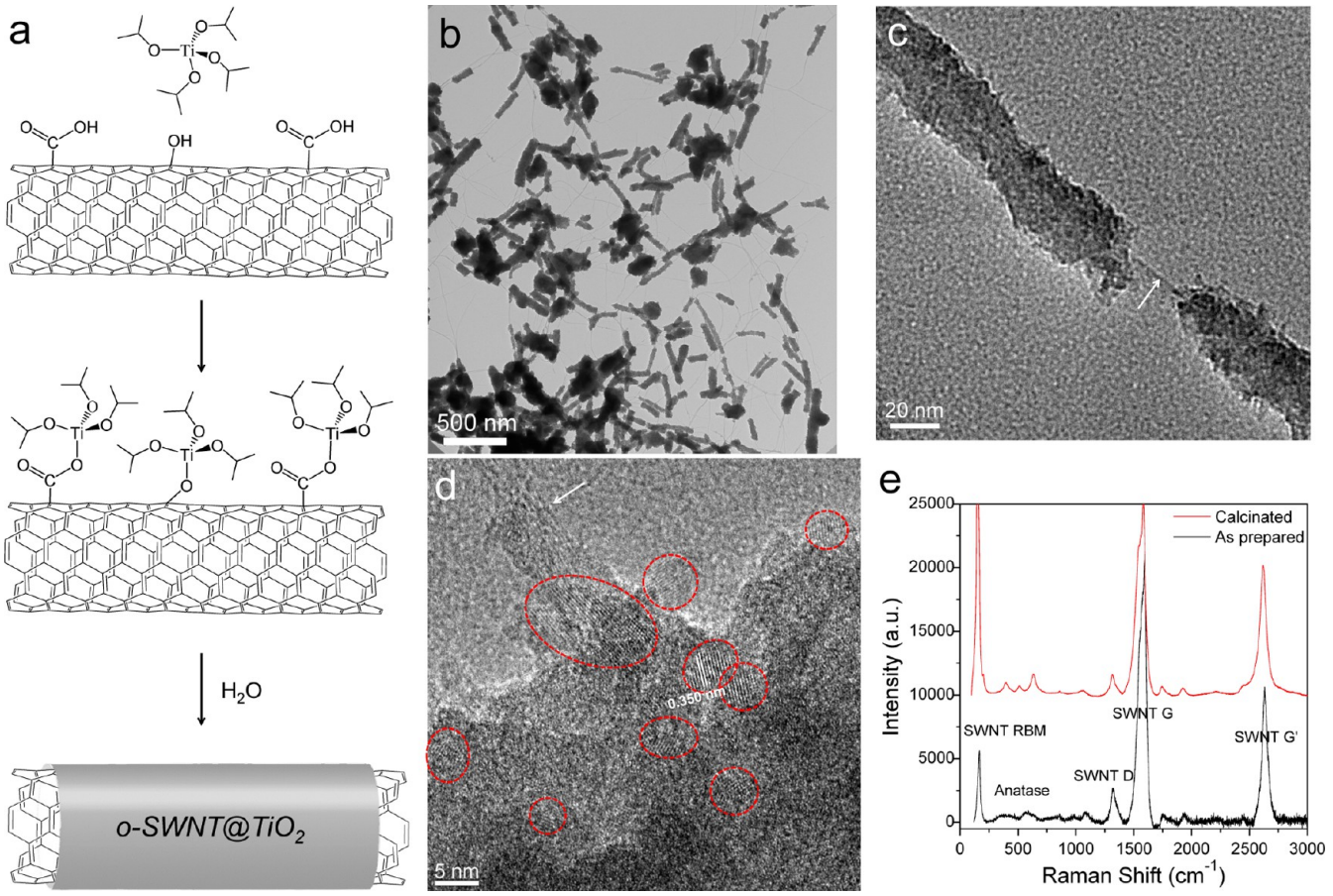

Figure 1. Synthesis of o-SWNT@TiO_2. (a) Sol–gel synthesis of o-SWNT@TiO_2 hybrid using titanium isopropoxide, $Ti(O^iPr)_4$ as a precursor and oxidized SWNTs as a template. The $Ti(O^iPr)_4$ precursor first reacted with oxygen surface functionalities of SWNTs and further hydrolysis upon addition of water resulted in the growth of a TiO_2 shell over SWNTs. (b,c) TEM images revealing the formation of pseudo-1-D TiO_2 shells over SWNTs. (d) HR-TEM image of the SWNT–TiO_2 boundary, with small crystalline regions highlighted by red ovals. White arrows in (c) and (d) indicate the uncoated SWNT segments. (e) Raman spectroscopy of the o-SWNT@TiO_2 hybrids before and after calcination.

ogy of this o-SWNT@TiO_2 core/shell hybrid material. Exposed parts of nanotubes were still observed (Figure 1c), indicating an incomplete TiO_2 layer on the SWNT surface determined by the distribution of oxygen functional groups on the nanotube walls. TiO_2 templated along o-SWNTs in a pseudo-1-D morphology, with some level of aggregations probably resulting from the hydrolysis and condensation of excess of $Ti(O^iPr)_4$ in the suspension. The majority part of as-synthesized TiO_2 appeared to be amorphous, with small crystalline regions observed in high-resolution TEM (HR-TEM) images (Figure 1d). The interfringe distances of the crystal lattice in these areas were determined to be 0.350 nm, which correspond to the lattice spacing of anatase (101) surface. Similar to other TiO_2 materials prepared by sol–gel approach, the overall cystallinity of the o-SWNT@TiO_2 nanohybrids could be tuned upon further calcination (Figure 1e). Raman spectroscopy, X-ray diffraction (XRD), and energy-dispersive X-ray spectroscopy (EDX) were employed to confirm the composition and crystallinity of the resulting nanostructures (see Figure S1). We also noticed that the thickness and morphology of the TiO_2 shell were dependent on the amount and rate of water injection during sol–gel synthesis with SWNT templates (Figure S2).

Electrical Behavior and Interfacial Charge Transfer of o-SWNT@TiO_2 Hybrid Under UV Illumination. As illustrated in Figure 2, a conductive film was fabricated via deposition of o-SWNT@TiO_2 hybrid on a Si wafer with SiO_2 insulating layer and interdigitated gold electrodes (10 μm pitch) prepared by standard photolithography (Figure 2a). Figure 2b,c depicts scanning electron microscopy (SEM) images of o-SWNT@TiO_2 hybrid network forming electrical connections between the gold electrodes. Upon illumination with ultraviolet light (365 nm), o-SWNT@TiO_2 hybrid networks showed a decrease in conductance, as demonstrated in Figure 2d. When the UV light was turned off, the conductance of o-SWNT@TiO_2 device only underwent a partial recovery, and the rate of conductance increase was much slower compared with the initial decrease in response to UV light (Figure 2d). The dramatic decrease in conductance is consistent with the previously reported phenomena of photoexcited electrons being transferred from the conduction band of TiO_2 to the conduction band of SWNTs.[7,15] Another possible phenomena, generation of the photocurrent in the TiO_2 component was ruled out in this case as it should result in an opposite signal (Figure S3). Since semiconducting-SWNTs demonstrated a typical p-type behavior at ambient conditions,[37] electron transfer to the SWNTs caused reduction of the hole carriers in SWNTs, leading to a decrease in the network conductivity. Such electron transfer has been known to allow a more effective charge separation in TiO_2 and consequently inhibit the electron–hole recombination. The prevention of fast recombination in TiO_2 is indeed observed from the relatively slow recovery of baseline conductance in Figure 2d. To further

dx.doi.org/10.1021/ja402887v | J. Am. Chem. Soc. 2013, 135, 9015–9022

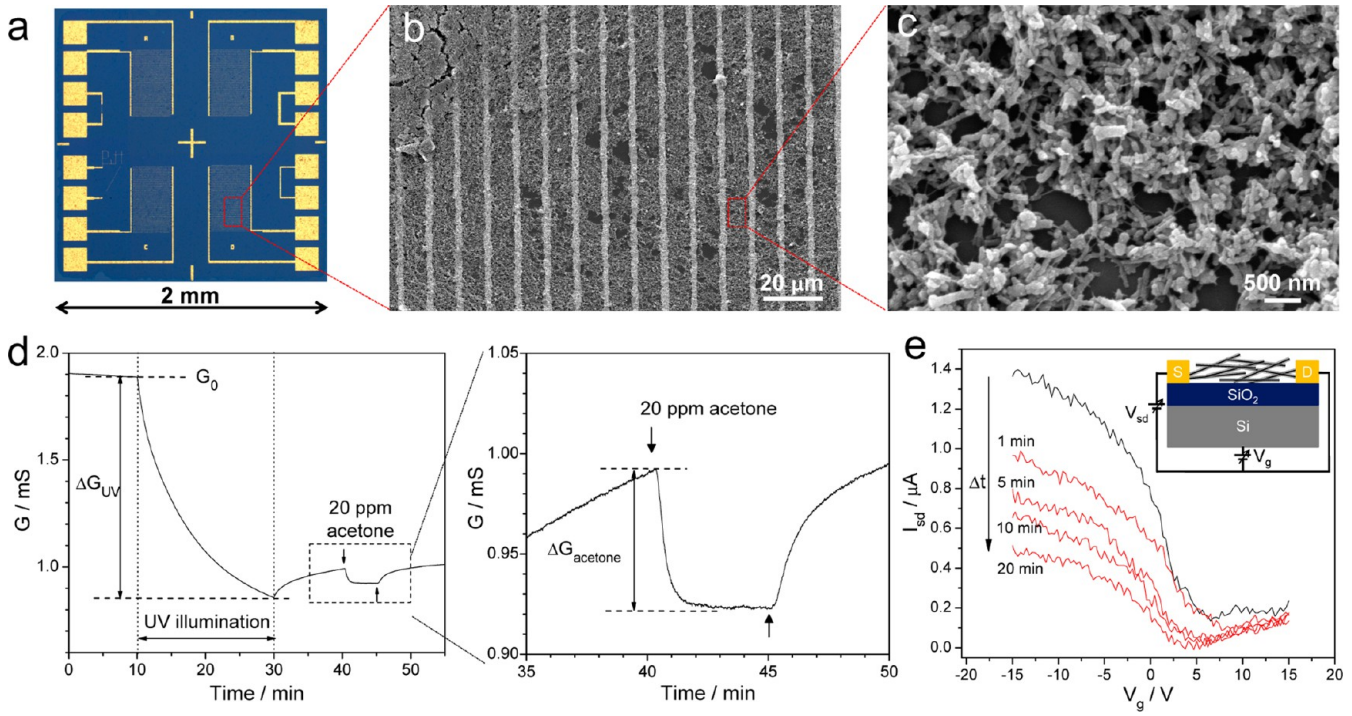

Figure 2. Electrical behavior of o-SWNT@TiO_2 devices under UV illumination and chemical exposure. (a) Optical image of a silicon chip with four sets of interdigitated gold electrodes used in this study. (b,c) SEM images of the o-SWNT@TiO_2 core/shell hybrid film deposited between the gold electrodes. (d) Conductance (G) versus time response to ultraviolet light (365 nm) illumination and acetone vapors (20 ppm, balanced in N_2). Arrows indicate beginning and end of acetone exposure. (e) FET characteristics of SWNT−TiO_2 hybrid network in N_2 under UV illumination at different time intervals (V_{sd} = 3 V). Inset: schematic representation of the o-SWNT@TiO_2 FET device.

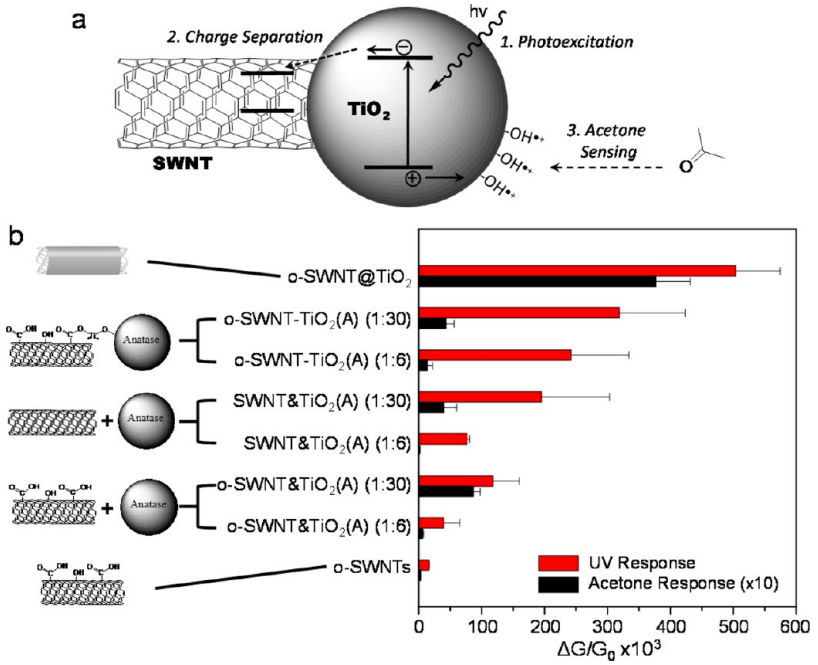

Figure 3. Schematic illustration of UV illumination, charge separation, and acetone sensing and comparison of the electrical responses of different SWNT−TiO_2 hybrid systems. (a) Schematic of the band structure of SWNT−TiO_2 hybrid, photoinduced charge separation, and acetone sensitivity. (b) Schematic illustrations (left) of different SWNT−TiO_2 hybrid systems including: oxidized SWNTs (o-SWNTs), as-prepared o-SWNT@TiO_2 core/shell hybrid, covalently linked anatase nanopowders with o-SWNTs (o-SWNT−TiO_2(A)), mechanically mixed pristine SWNTs and anatase nanopowders (SWNT&TiO_2(A)), and mechanically mixed o-SWNTs and anatase nanopowders (o-SWNT&TiO_2(A)). The numbers after each label indicate the weight ratio of SWNTs to TiO_2 in the hybrid. The right panel illustrates the UV (red bars) and acetone responses (black bars) of each hybrid system, with standard deviation (n = 15). For comparison, acetone responses were multiplied by a factor of 10.

probe this process, similar measurements were done on the SWNT−TiO_2 devices in the presence of oxygen (air). A relatively slower conductance drop in response to the UV illumination was observed in the air environment, and the

dx.doi.org/10.1021/ja402887v | J. Am. Chem. Soc. 2013, 135, 9015−9022

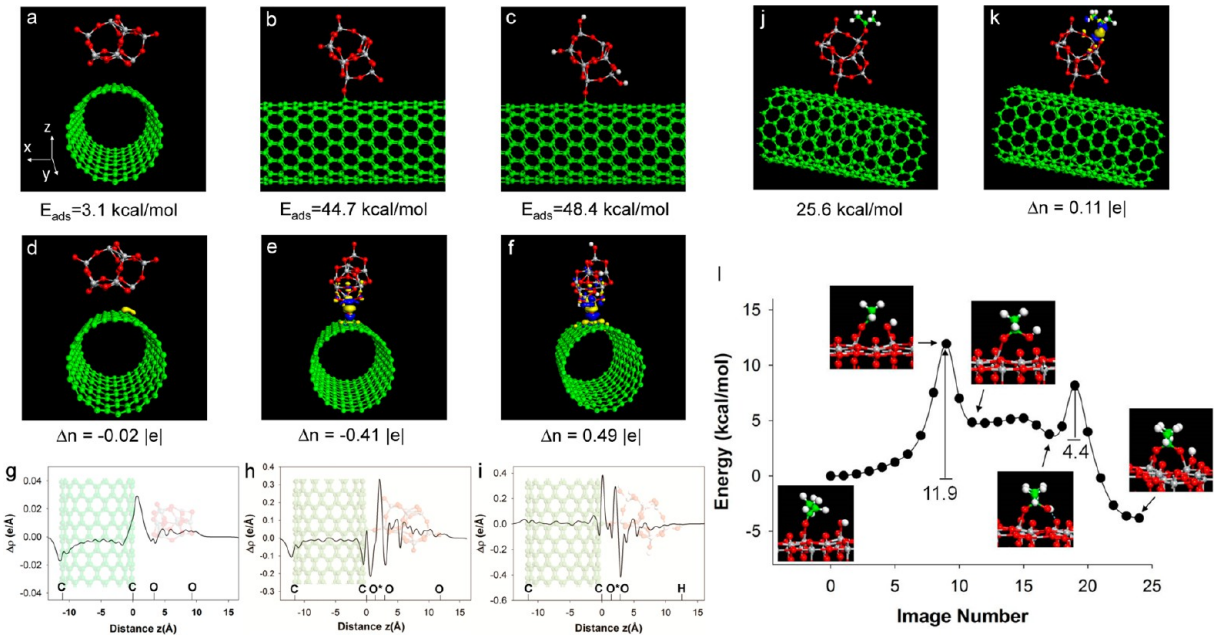

Figure 4. DFT simulation of the electronic coupling and acetone sensing process. (a) Representative adsorption configuration of a $Ti_{10}O_{20}$ cluster on a pristine (14,0) SWNT. (b) Adsorption configuration of a $Ti_{10}O_{20}$ cluster on a (14,0) SWNT through Ti−O−C linkage. (c) Adsorption of a hydrogenated (with formation of four OH bonds) $Ti_{10}O_{20}$ cluster on the oxygen-decorated SWNT. C atoms are green, Ti atoms are gray, O atoms are red, and H atoms are white. The adsorption energies (E_{ads}) of $Ti_{10}O_{20}$ cluster are indicated for each case in the lower part of the top panels. (d−f) Charge difference maps of the $Ti_{10}O_{20}$ cluster for the binding configurations illustrated in panels a−c, respectively. The corresponding Bader charges (Δn) transferred from SWNT (with O in e and f) to $Ti_{10}O_{20}$ are shown in each case. In panel d the indicated isosurfaces correspond to values of 0.004 $e^-/Å^3$ (yellow) and −0.0015 $e^-/Å^3$ (blue) while in panels e and f to values of +0.02 $e^-/Å^3$ (yellow) and −0.02 $e^-/Å^3$ (blue). (g−i) Plane averaged charge density different plots for configurations (a−c) at different z-planes, respectively. (j) Adsorption configuration of acetone on-top of a Ti site (η^1-acetone) on the SWNT−O-$Ti_{10}O_{20}$ hybrid and the corresponding E_{ads}. (k) Charge difference map of acetone for the binding configurations in panel j and corresponding Bader charge transfer from acetone to $Ti_{10}O_{20}$ cluster. (l) Minimum energy pathway for reaction of a η^1-acetone molecule initially coadsorbed near a terminal hydroxyl OH_t group on anatase (101) surface leading to formation of a $(CH_3)_2CO$−OH complex (configuration nos. 11 and 17) followed by transfer of a H atom to a surface bridging oxygen and formation of an η^2-acetone−O adatom complex (configuration no. 24).

recovery was much faster (Figure S4a). The slower UV response and faster recovery in air are in accordance with the addition of electron scavengers (oxygen adsorbed on TiO_2 surface) in the oxygen-rich environment that can trap the photoexcited electrons[38,39] and subsequently limit their transfer to SWNTs. This quenching effect was further supported by the conductance recovery observed during the 20% oxygen exposure when SWNT/TiO_2 device was under the UV illumination (Figure S4b).

The o-SWNT@TiO_2 hybrid network was also tested in a field-effect transistor (FET) device configuration using interdigitated gold electrodes as source/drain and a Si substrate as back gate. As shown in Figure 2e, o-SWNT@TiO_2 hybrid demonstrated p-type FET characteristics, similar to the random network composed of pristine SWNTs at ambient conditions.[37,40] This indicates that the transistor characteristics of the hybrid are determined by SWNT components. Upon UV illumination, the $I-V_g$ curve of SWNT−TiO_2 tilted and shifted to a negative gate voltage (negative threshold voltage) and a smaller current. The change in FET characteristics at zero gate voltage matches the conductance versus time measurements (Figure 2d). A shift toward negative gate voltage generally indicates a decrease in hole carrier concentration for the p-type semiconductor after UV exposure. This is also consistent with the charge transfer from excited TiO_2 to semiconducting SWNTs. Due to the presence of metallic SWNTs, the SWNT−TiO_2 network also demonstrated a baseline conductance when the transistor was adjusted to the "off state". The decrease in current that was simultaneously observed upon UV illumination suggests creation of scattering centers at the SWNT−TiO_2 interface that influence the conductivity of metallic SWNTs as well. The emerged ambipolar characteristic of the SWNT−TiO_2 transistor is another consequence of the reduction of hole carriers and is in accordance with similar studies on the bare SWNT devices.[41] The summarized process of photoexcitation and subsequent electron transfer is illustrated in Figure 3a.

Photoinduced Electrical Sensitivity to Acetone Molecules. Chemical sensitivity provides useful information on the process of surface adsorption[37,42] and catalytic reactions.[37,38] Moreover, it also characterizes the potential of hybrid materials for practical application in chemical detection. When the UV light was turned off, the slowly recovering conductance of SWNT−TiO_2 went close to a steady state after 10 min in N_2 and set up a new baseline that could be utilized for chemical sensitivity tests. As shown in Figure 2d, exposure to 20 ppm acetone vapors led to a fast decrease in the conductance of o-SWNT@TiO_2 device, with complete recovery to the baseline when acetone vapor exposure was terminated (for higher concentrations, see Figure S5). This photoinduced acetone sensitivity is different from previously reported sensors based on CNTs[37,43−45] and provides useful information on the molecular interactions between nanohybrid and acetone molecules with implications for future development of acetone sensors and catalysts for the photooxidation of acetone.

Charge-Transfer Efficiency and Acetone Reactivity of the Photoexcited Hybrid Systems. In order to confirm our

dx.doi.org/10.1021/ja402887v | J. Am. Chem. Soc. 2013, 135, 9015−9022

proposed interfacial process in the SWNT−TiO_2 hybrids and to better understand the factors that regulate their electrical behavior, other SWNT−TiO_2 hybrid systems with different morphologies and interface conditions were also synthesized and analyzed. Specifically, commercially available pristine or oxidized SWNTs and anatase TiO_2(A) samples were mixed by either mechanical mixing (using sonication) or covalent attachment (see Experimental Section for details). Similar electrical measurements were performed on all these SWNT−TiO_2 hybrid systems, and their UV and acetone responses (defined in Figure 2d) are summarized in Figure 3b.

First, it could be noticed that addition of TiO_2 dramatically increased the UV response of the device compared with bare SWNTs network (either pristine or oxidized SWNTs), and larger UV responses were observed for a higher amount of TiO_2 in all hybrid systems, regardless of their interconnections with SWNTs. Such difference in the magnitude of conductance change and its correlation with the TiO_2 loading further confirmed that the electrical behavior of SWNT−TiO_2 hybrid systems was a result of the interfacial charge-transfer process, different from the photoinduced molecular desorption mechanism previously proposed for bare SWNTs devices.[41,46,47] Moreover, while pristine SWNTs and oxidized SWNTs showed similar UV and acetone sensitivities when mechanically mixed with anatase TiO_2(A) nanocrystals, covalent attachment between TiO_2 nanocrystals and SWNTs led to a significant increase in the UV response (o-SWNT@TiO_2(A) vs o-SWNT−TiO_2(A) in Figure 3b). This difference clearly indicates that covalent linkage between TiO_2 and SWNTs led to enhanced electron-transfer efficiency and therefore a better charge-hole separation in the hybrid system, while the type of SWNTs (pristine vs oxidized) had less influence. Overall, o-SWNT@TiO_2 presented the largest UV response, because of increased covalent linkage and interface area between SWNT and TiO_2. We can conclude from all these results that this hybrid system presents an efficient electronic transfer at interface upon UV irradiation.

Increasing the amount of TiO_2 resulted in enhanced acetone sensitivity in all nanohybrid systems, which confirmed its role of recognition layer (Figure 3b). Compared with other hybrid systems, o-SWNT@TiO_2 core/shell hybrid demonstrated the highest acetone sensitivity, which is probably due to two distinct factors: (i) The abundant covalent bonding between SWNTs and TiO_2 facilitates the electronic coupling and interactions across the hybrid interface, leading to a more efficient and sensitive interfacial charge transfer (as also indicated by its best UV response); and (ii) the less ordered structure of as-synthesized TiO_2 (amorphous in nature with few small crystalline areas) offers more oxygen vacancies or unsaturated surface Ti centers that were more reactive to acetone molecules, as compared to the highly crystallized commercial TiO_2 nanoparticles (Figure 3b).

Theoretical Simulations of the SWNT−TiO_2 Interaction and Acetone Sensing. The main findings on the charge transfer efficiency and acetone sensitivity of different SWNT−TiO_2 hybrid systems obtained by electrical measurements were further supported by density functional theory (DFT) calculations. Figure 4a depicts the optimized binding configuration of a $Ti_{10}O_{20}$ cluster on a pristine (14,0)-SWNT surface, while Figure 4b,c illustrates the adsorption of the same cluster, respectively, of a hydrogenated TiO_2 cluster on a SWNT functionalized with an O atom with formation of a covalent Ti−O−C linkage. For each of these configurations, corresponding binding energies of the $Ti_{10}O_{20}$ ($Ti_{10}O_{20}H_4$) cluster on SWNT are also indicated. The interfacial charge distributions (with the calculated amount of electron transfer) and the charge differential plots are also listed in Figure 4d−f and g−i, respectively. A negligible binding energy and very small charge transfer between the TiO_2 cluster and the pristine SWNT (Figure 4a,d,g) indicated weak mutual interactions. This interaction was significantly increased upon formation of a covalent linkage facilitated by the presence of either adsorbed O (44.7 kcal/mol in Figure 4b vs 3.1 kcal/mol in Figure 4a) or COOH groups (Figure S6), with direct enhancement of the interfacial charge transfer (−0.41 e in Figure 4e vs −0.02 e in Figure 4d). The enhanced interfacial electronic coupling (also see Figure 4h) through covalent linkage is also in agreement with UV response measurements. Furthermore, hydrogenation of the $Ti_{10}O_{20}$ cluster showed a significant influence on the charge distribution at the hybrid interface (Figure 4f,i), indicating the sensitivity of the interfacial charge distribution within the SWNT−TiO_2 nanohybrids upon binding of any redox chemical species on the surface active site.

We further analyzed the adsorption of an acetone molecule on the TiO_2 cluster. A representative binding configuration and the corresponding charge transfer at the acetone−oxide interface are illustrated in Figure 4j,k. An electron transfer of 0.11 e from acetone to the hybrid was observed (Figure 4k), indicating a partial oxidation of the acetone molecule, which explained the observed reduction of the hole carriers of the p-type SWNT/TiO_2 hybrids (Figure 2). We further assume that the effect of UV illumination was to generate enough reactive sites for acetone molecules on the TiO_2 surface (such as hydroxyl radicals) that were probably occupied by other molecules (such as water) before the UV exposure. Furthermore, several possible intermediate configurations from the reaction between an adsorbed acetone (in a η_1-configuration at a Ti five-folded site) and a nearby terminal hydroxyl (OH_t) group (that mimics the hydroxyl radical generated through UV illumination) on the TiO_2 anatase (101) surface were calculated and their minimum energy reaction profile is shown in Figure 4l. We observed relative low-energy barriers for both the direct and reverse reactions of acetone−OH_t and formation of acetone−O adatom complex. This behavior is consistent to the observed reversible electrical signals in the sensor tests. In particular, for the acetone−O adatom configuration a new band in the density of states was observed within the band gap of TiO_2 (Figure S7). This intermediate band indicated that adsorbed acetone molecules could further serve as hole traps on the photoexcited TiO_2 surface and could be further oxidized if under continuous UV illumination. As a comparison, the reaction energy for an irreversible dissociation of the adsorbed acetone was also calculated (Figure S8). These theoretical results are also consistent with our observations that during the sensing measurements, the response of SWNT−TiO_2 device was actually irreversible if the UV light was kept on (Figure S5). This irreversible detection with *in situ* UV exposure was indeed a result of the irreversible oxidation of the adsorbed acetone on the photoexcited TiO_2. The overall mechanism of photoinduced acetone sensitivity of SWNT−TiO_2 indicated by the experimental and theoretical results is also summarized in Figure 3a.

Acetone Sensing with o-SWNT@TiO_2 and Its Potential in the Breath Detection. The photoinduced acetone sensitivity of o-SWNT@TiO_2 hybrid can be utilized as a

dx.doi.org/10.1021/ja402887v | J. Am. Chem. Soc. 2013, 135, 9015−9022

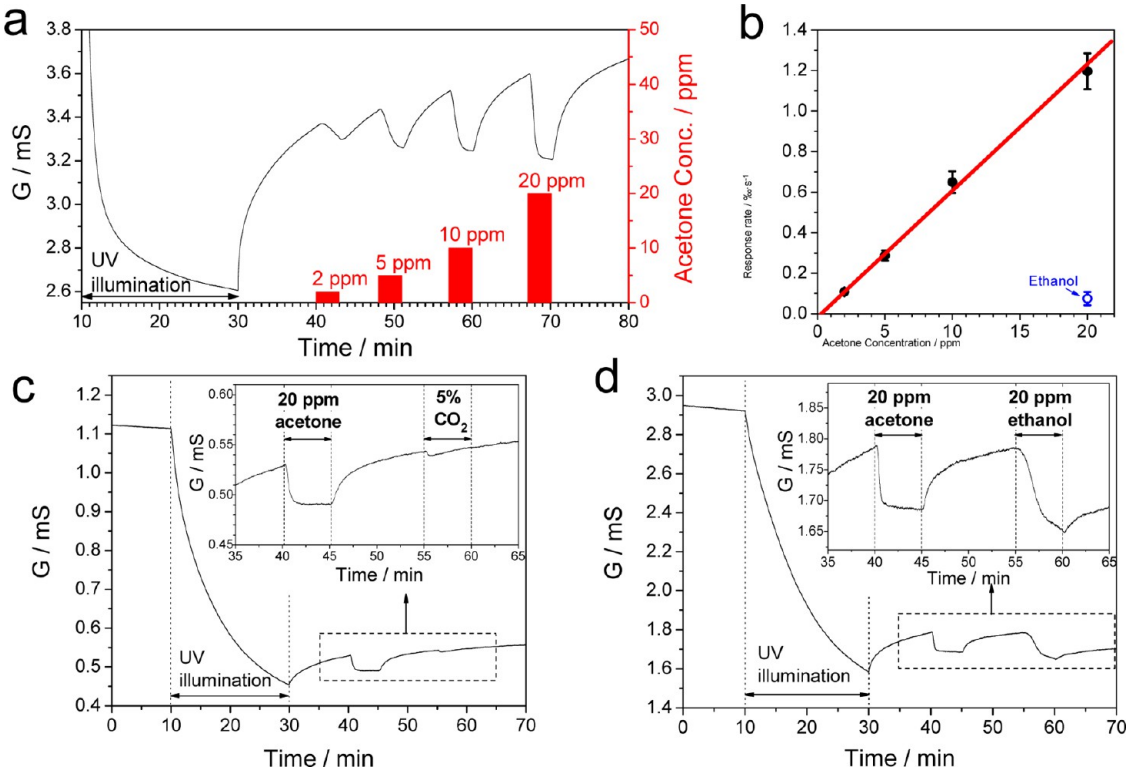

Figure 5. Electrical response of o-SWNT@TiO_2 devices to varying acetone concentrations. (a) Conductance (G) response of the device to acetone vapors of varying concentrations (2, 5, 10, and 20 ppm, balanced in N_2) after UV illumination. (b) Acetone response rate (i.e., relative conductance change per unit time) of o-SWNT@TiO_2 devices (n = 10). (c,d) Cross sensitivity of the o-SWNT@TiO_2 device between 20 ppm acetone and 5% CO_2 (c) 20 ppm ethanol (d).

promising sensory tool for the electrical detection of acetone vapors. Figure 5a depicts the electrical response of o-SWNT@TiO_2 devices (in a chemiresistor configuration) upon exposure to varying concentrations of acetone vapors at ppm level. The baseline of the sensor device was first set up through UV illumination, and four pulses of acetone vapors (diluted with N_2) with increasing concentrations (indicated by red bars) were subsequently introduced into the gas flow cell. As shown in Figure 5a, multiple exposures were successfully measured as each electrical response reached a full recovery after respective pulses without any additional operation (for device variations, see Figure S9). Different response rates were also observed to the varying concentration of acetone vapors. The response signal did not saturate at lower concentration (2 ppm) during the 180 s of each acetone exposure, but the device reached equilibrium in a shorter time at higher concentrations (t_{90} = 50 s for 20 ppm). We found a linear relationship between the electrical response rate at the first 60 s (fast response region) and the acetone concentrations, which could serve as calibration curve for the sensor (Figure 5b). For 180 s of exposure time, we calculated a signal-to-noise ratio (S/N) of 14 for 2 ppm of acetone, and a detection limit of 0.4 ppm was determined (using S/N = 3) for our o-SWNT@TiO_2 acetone sensor. This detection limit is lower compared with previously reported SWNT-based detection of acetone,[37,43,44] which is limited by its weak electronic interactions with SWNTs.[45] Although utilizing TiO_2 as a sensitive coating to CNTs has been previously reported,[48] our results demonstrate that the photoexcited o-SWNT@TiO_2 has improved sensitivity to acetone.

To evaluate the potential of these acetone sensors for breath analysis, cross-sensitivity tests to major components of human breath (O_2, CO_2, H_2O, and ethanol) and other possible breath biomarkers (NH_3, H_2, CO, and NO)[35,49,50] were also performed. We did not observe any significant response when o-SWNT@TiO_2 was exposed to 5% CO_2, as shown in Figure 5c. The negligible CO_2 response of o-SWNT@TiO_2 is in accordance with the low binding energy and reactivity of CO_2 molecules on the TiO_2 surface.[51] For a similar reason, no significant cross-sensitivity was observed for other trace biomarkers, indicating a potentially selective detection of breath acetone using o-SWNT@TiO_2 if other metabolic conditions exist (Figure S10). We have already demonstrated that O_2 had a larger effect on the excited o-SWNT@TiO_2 as electron scavenger, and cross-sensitivity to humidity vapor was also observed due to its molecular interaction with both TiO_2 and SWNTs (Figure S4b,c). Despite its sensitivity to O_2 and H_2O, the o-SWNT@TiO_2 sensor was successfully utilized to detect 20 ppm of acetone vapor in both air and a high humidity background, although with increased noise level and higher detection limit (Figure S4d). Ethanol is another type of hole scavenger and could be present in human breath as a result of the alcohol consumption. As shown in Figure 5d, photoexcited o-SWNT@TiO_2 demonstrated a comparable sensitivity yet a different response dynamic toward 20 ppm acetone and ethanol vapors. This result indicated different types of adsorption or reaction occurred on the photoexcited TiO_2 surface for these two analytes (Figure S11). Due to the different response dynamics, electrical response of o-SWNT@TiO_2 to acetone and ethanol vapors with comparable concentrations can be distinguished via their response rates (as demonstrated in

dx.doi.org/10.1021/ja402887v | J. Am. Chem. Soc. 2013, 135, 9015−9022

Figure 5b). For practical sensor considerations, our results indicate that high concentrations of alcohol vapors in human breath could result in false positives during the analysis of breath acetone and cautions or additional steps have to be taken in such cases.

CONCLUSION

In summary, we have developed facile and scalable synthesis of the o-SWNT@TiO_2 hybrid nanostructures with controlled core/shell morphology. Unique electrical behavior of this hybrid nanomaterial was observed in response to the UV illumination and subsequent chemical exposure. Based on both experimental and theoretical studies of a group of systematically designed SWNT−TiO_2 hybrid systems, we established a fundamental understanding of interfacial charge transfers between photoexcited TiO_2 and SWNTs with different morphologies and interfacial conditions. The ability to monitor the efficiency of electron−hole separation during the UV excitation with the SWNTs as an electrical probe would benefit the future design and development of SWNT−TiO_2 based photovoltaic devices or photocatalysts.

Utilizing the o-SWNT@TiO_2 devices as chemiresistors, we demonstrated ultrahigh acetone sensitivities with linear and reversible responses at the concentration range between 2 and 20 ppm and a calculated detection limit of 0.4 ppm. The ultrahigh sensitivity to ppm level of acetone vapors, fast and reversible response, together with miniature size and room temperature operation makes this o-SWNT@TiO_2 nanohybrid a promising sensing platform that could find applications in the detection of breath acetone. The development of a microsized low-power electronic breath acetone sensor device could further benefit personal healthcare by serving as a convenient and low-cost diagnostic tool for diabetes or a novel and high-throughput analytical method in the clinical studies of metabolic disorders.

EXPERIMENTAL SECTION

Synthesis of o-SWNT@TiO_2 Core/Shell Hybrid. o-SWNTs (0.5 mg) were suspended in ethanol (17 mL) by ultrasonication (30 min using a Branson 5510 bath sonicator). $Ti(O^iPr)_4$ (50 μL) was added under vigorous stirring using micropipet and the mixture of o-SWNTs and $Ti(O^iPr)_4$ was stirred for 1 h. Deionized (DI) water was subsequently added into the system (300 μL × 10 over 50 min), and the resulting mixture was stirred for an additional 15 min. The final product was isolated on a filter (PTFE filter membrane, 2 μm), washed with ethanol (×3), and resuspended in DI water (20 mL).

General Characterizations. TEM of all the synthesized samples were performed on a FEI Morgagni microscope, operating at an acceleration voltage of 80 keV. High-resolution TEM (HRTEM) images were obtained on a JEOL 2010F high-resolution transmission electron microscope, operating at an accelerating voltage of 200 keV. Scanning electron microscopy (SEM) was performed with a Phillips XL30 FEG microscope equipped with an energy dispersive X-ray spectroscopy accessory. XRD was performed with a Bruker D8 Discover XRD with GADDS Detector for powder and thin film diffraction. Raman spectroscopy was performed with a Renishaw inVia Micro-Raman Microscope (using an excitation wavelength of 633 nm).

Electrical Test and Chemical Sensing Measurement. Si chips with an oxide layer (300 nm thick) and interdigitated gold electrodes were purchased from MEMS and Nanotechnology Exchange. The devices were fabricated by dropcasting aqueous suspension (3 μL) of SWNT−TiO_2 hybrids onto the Si chips which were connected to the 40 CERDIP packages with Au wires and allowed to dry in ambient conditions. Electrical tests and gas sensing measurements were conducted using a custom-made system.[10,11] SWNT−TiO_2 devices were placed in a sealed Teflon chamber to control the gas environment, and their electrical conductance was measured (bias voltage: 500 mV) on a test board by Keithley Dual SourceMeter 2602 and Keithley Switching Matrix 708A (4 data output simultaneously), controlled by a Zephyr data-acquisition software (http://zephyr.sourceforge.net). Ultraviolet light was generated from a UVP Model UVGL-55 hand-held lamp (365 nm in wavelength, 25 $\mu W \cdot cm^{-2}$). During the sensing tests, different concentrations of analyte gases were generated by mixing certified gases (20 ppm acetone balanced in dry N_2, and other gases all purchased from Valley National Gas, Inc.) with dry N_2 at controlled ratio of gas flow rate and were passed through the gas chamber containing the sensor device.

ASSOCIATED CONTENT

Supporting Information

Additional experimental and computational methods, characterizations, electrical tests, and discussion. This material is available free of charge via the Internet at http://pubs.acs.org.

AUTHOR INFORMATION

Corresponding Author

astar@pitt.edu

Notes

The authors declare no competing financial interest.

ACKNOWLEDGMENTS

This work was performed in support of ongoing research in sensor systems and diagnostics at the National Energy Technology Laboratory (NETL) under URS contract DE-FE0004000.

REFERENCES

(1) Yan, H.; Choe, H. S.; Nam, S.; Hu, Y.; Das, S.; Klemic, J. F.; Ellenbogen, J. C.; Lieber, C. M. *Nature* **2011**, *470*, 240−244.
(2) Siegwart, D. J.; Whitehead, K. A.; Nuhn, L.; Sahay, G.; Cheng, H.; Jiang, S.; Ma, M.; Lytton-Jean, A.; Vegas, A.; Fenton, P.; Levins, C. G.; Love, K. T.; Lee, H.; Cortez, C.; Collins, S. P.; Li, Y. F.; Jang, J.; Querbes, W.; Zurenko, C.; Novobrantseva, T.; Langer, R.; Anderson, D. G. *Proc. Natl. Acad. Sci. U.S.A.* **2011**, *108*, 12996−13001.
(3) Ambrogio, M. W.; Thomas, C. R.; Zhao, Y.-L.; Zink, J. I.; Stoddart, J. F. *Acc. Chem. Res.* **2011**, *44*, 903−913.
(4) Sailor, M. J.; Park, J. H. *Adv. Mater.* **2012**, *24*, 3779−802.
(5) Joo, S. H.; Park, J. Y.; Tsung, C.-K.; Yamada, Y.; Yang, P.; Somorjai, G. A. *Nat. Mater.* **2009**, *8*, 126−131.
(6) Yamada, Y.; Tsung, C.-K.; Huang, W.; Huo, Z.; Habas, S. E.; Soejima, T.; Aliaga, C. E.; Somorjai, G. A.; Yang, P. *Nat. Chem.* **2011**, *3*, 372−376.
(7) Dang, X.; Yi, H.; Ham, M.-H.; Qi, J.; Yun, D. S.; Ladewski, R.; Strano, M. S.; Hammond, P. T.; Belcher, A. M. *Nat. Nanotechnol.* **2011**, *6*, 377−384.
(8) Kempa, T. J.; Cahoon, J. F.; Kim, S.-K.; Day, R. W.; Bell, D. C.; Park, H.-G.; Lieber, C. M. *Proc. Natl. Acad. Sci. U.S.A.* **2012**, *109*, 1407−1412.
(9) Rosi, N. L.; Mirkin, C. A. *Chem. Rev.* **2005**, *105*, 1547−1562.
(10) Kauffman, D. R.; Shade, C. M.; Uh, H.; Petoud, S.; Star, A. *Nat. Chem.* **2009**, *1*, 500−506.
(11) Ding, M.; Sorescu, D. C.; Kotchey, G. P.; Star, A. *J. Am. Chem. Soc.* **2012**, *134*, 3472−3479.
(12) Ding, M.; Tang, Y.; Gou, P.; Reber, M. J.; Star, A. *Adv. Mater.* **2011**, *23*, 536−540.
(13) Woan, K.; Pyrgiotakis, G.; Sigmund, W. *Adv. Mater.* **2009**, *21*, 2233−2239.
(14) Kongkanand, A.; Martínez Domínguez, R.; Kamat, P. V. *Nano Lett.* **2007**, *7*, 676−680.
(15) Yao, Y.; Li, G.; Ciston, S.; Lueptow, R. M.; Gray, K. A. *Environ. Sci. Technol.* **2008**, *42*, 4952−4957.

(16) Lee, W. J.; Lee, J. M.; Kochuveedu, S. T.; Han, T. H.; Jeong, H. Y.; Park, M.; Yun, J. M.; Kwon, J.; No, K.; Kim, D. H.; Kim, S. O. *ACS Nano* **2011**, *6*, 935−943.
(17) Hsu, C.-Y.; Lien, D.-H.; Lu, S.-Y.; Chen, C.-Y.; Kang, C.-F.; Chueh, Y.-L.; Hsu, W.-K.; He, J.-H. *ACS Nano* **2012**, *6*, 6687−6692.
(18) Cargnello, M.; Grzelczak, M.; Rodríguez-González, B.; Syrgiannis, Z.; Bakhmutsky, K.; La Parola, V.; Liz-Marzán, L. M.; Gorte, R. J.; Prato, M.; Fornasiero, P. *J. Am. Chem. Soc.* **2012**, *134*, 11760−11766.
(19) Law, M.; Greene, L. E.; Johnson, J. C.; Saykally, R.; Yang, P. *Nat. Mater.* **2005**, *4*, 455−459.
(20) Hochbaum, A. I.; Yang, P. *Chem. Rev.* **2009**, *110*, 527−546.
(21) Hoang, S.; Guo, S.; Hahn, N. T.; Bard, A. J.; Mullins, C. B. *Nano Lett.* **2011**, *12*, 26−32.
(22) Hu, A.; Liu, S.; Lin, W. *RSC Adv.* **2012**, *2*, 2576−2580.
(23) Hoang, S.; Berglund, S. P.; Hahn, N. T.; Bard, A. J.; Mullins, C. B. *J. Am. Chem. Soc.* **2012**, *134*, 3659−3662.
(24) Feng, X.; Zhu, K.; Frank, A. J.; Grimes, C. A.; Mallouk, T. E. *Angew. Chem., Int. Ed.* **2012**, *51*, 2727−30.
(25) Hwang, Y. J.; Boukai, A.; Yang, P. *Nano Lett.* **2008**, *9*, 410−415.
(26) Xu, C.; Wu, J.; Desai, U. V.; Gao, D. *Nano Lett.* **2012**, *12*, 2420−2424.
(27) D'Souza, F.; Chitta, R.; Sandanayaka, A. S. D.; Subbaiyan, N. K.; D'Souza, L.; Araki, Y.; Ito, O. *J. Am. Chem. Soc.* **2007**, *129*, 15865−15871.
(28) Ehli, C.; Oelsner, C.; Guldi, D. M.; Mateo-Alonso, A.; Prato, M.; Schmidt, C.; Backes, C.; Hauke, F.; Hirsch, A. *Nat. Chem.* **2009**, *1*, 243−249.
(29) Oelsner, C.; Herrero, M. A.; Ehli, C.; Prato, M.; Guldi, D. M. *J. Am. Chem. Soc.* **2011**, *133*, 18696−18706.
(30) Oelsner, C.; Schmidt, C.; Hauke, F.; Prato, M.; Hirsch, A.; Guldi, D. M. *J. Am. Chem. Soc.* **2011**, *133*, 4580−4586.
(31) Ding, M.; Tang, Y.; Star, A. *J. Phys. Chem. Lett.* **2012**, *4*, 147−160.
(32) Hu, L.; Zhao, Y. L.; Ryu, K.; Zhou, C.; Stoddart, J. F.; Grüner, G. *Adv. Mater.* **2008**, *20*, 939−946.
(33) Liu, S.; Li, J.; Shen, Q.; Cao, Y.; Guo, X.; Zhang, G.; Feng, C.; Zhang, J.; Liu, Z.; Steigerwald, M. L.; Xu, D.; Nuckolls, C. *Angew. Chem., Int. Ed.* **2009**, *48*, 4759−4762.
(34) Laffel, L. *Diabetes/Metab. Res. Rev.* **1999**, *15*, 412−426.
(35) Cao, W.; Duan, Y. *Clin. Chem.* **2006**, *52*, 800−811.
(36) Itkis, M. E.; Perea, D. E.; Niyogi, S.; Rickard, S. M.; Hamon, M. A.; Hu, H.; Zhao, B.; Haddon, R. C. *Nano Lett.* **2003**, *3*, 309−314.
(37) Snow, E. S.; Perkins, F. K. *Nano Lett.* **2005**, *5*, 2414−2417.
(38) Thompson, T. L.; Yates, J. T. *Chem. Rev.* **2006**, *106*, 4428−4453.
(39) Bahnemann, D. W.; Hilgendorff, M.; Memming, R. *J. Phys. Chem. B* **1997**, *101*, 4265−4275.
(40) Snow, E. S.; Perkins, F. K.; Robinson, J. A. *Chem. Soc. Rev.* **2006**, *35*, 790−798.
(41) Chen, R. J.; Franklin, N. R.; Kong, J.; Cao, J.; Tombler, T. W.; Zhang, Y.; Dai, H. *Appl. Phys. Lett.* **2001**, *79*, 2258.
(42) Robinson, J. A.; Snow, E. S.; Badescu, S. C.; Reinecke, T. L.; Perkins, F. K. *Nano Lett.* **2006**, *6*, 1747−1751.
(43) Snow, E. S.; Perkins, F. K.; Houser, E. J.; Badescu, S. C.; Reinecke, T. L. *Science* **2005**, *307*, 1942−1945.
(44) Robinson, J. T.; Perkins, F. K.; Snow, E. S.; Wei, Z.; Sheehan, P. E. *Nano Lett.* **2008**, *8*, 3137−3140.
(45) Chakrapani, N.; Zhang, Y. M.; Nayak, S. K.; Moore, J. A.; Carroll, D. L.; Choi, Y. Y.; Ajayan, P. M. *J. Phys. Chem. B* **2003**, *107*, 9308−9311.
(46) Collins, P. G.; Bradley, K.; Ishigami, M.; Zettl, A. *Science* **2000**, *287*, 1801−1804.
(47) Chen, G.; Paronyan, T. M.; Pigos, E. M.; Harutyunyan, A. R. *Sci. Rep.* **2012**, *2*, 343.
(48) Guirado-López, R. A.; Sánchez, M.; Rincón, M. E. *J. Phys. Chem. C* **2006**, *111*, 57−65.
(49) Kharitonov, S. A.; Barnes, P. J. *Biomarkers* **2002**, *7*, 1−32.
(50) Wang, C.; Sahay, P. *Sensors* **2009**, *9*, 8230−8262.
(51) Lee, J.; Sorescu, D. C.; Deng, X. *J. Am. Chem. Soc.* **2011**, *133*, 10066−10069.